

X-ray standing waves: a method for thin layered systems

Markus Krämer,^{*a} Alex von Bohlen,^a Christian Sternemann,^b Michael Paulus^b and Roland Hergenröder^a

Received 22nd May 2006, Accepted 31st July 2006

First published as an Advance Article on the web 23rd August 2006

DOI: 10.1039/b607252f

X-ray standing wave spectroscopy at grazing incidence (GI-XSW) is demonstrated to be a versatile method to characterize multilayer thin films and element distributions on a nanometre scale. In this work we present a measurement procedure and development of a computerized simulation tool to interpret measured intensities. Four different kinds of samples are investigated. First, thickness determination of a set of thin germanium layers on silicon ranging from 29 nm to 1 μm is presented, which demonstrates the wide dynamic range that is feasible and the limitations that occur. Second, analysis of a sample of gold clusters evaporated on an 80 nm polystyrene film on a silicon substrate is shown. Low contrast organic mono-, double or multilayers is the third kind of sample to be characterized by XSW. Finally, qualitative and quantitative characterization of a laser multilayer mirror utilizing XSW and a fast Fourier transform evaluation method are described. Measurement and simulation procedures for each kind of sample are outlined in this report as well as the possibilities and limits of this XSW method.

Introduction

Thin films and multilayers have become very important in science and technology during the last decades. The semiconductor industry, laser and X-ray optics or organic surface modifications are a few of many application fields for these structures. Thus, measurement methods for thin films in the nanometre range are increasingly required. Also, polymers as well as metal-organic compounds are playing an important role in industry and science, *e.g.* in automobile production or as coatings of mass storage devices like CDs and DVDs.^{1–3}

Depending on the type of sample to be characterized, different measurement techniques from a wide variety of tools are available. However, besides already existing powerful methods, such as X-ray photoelectron spectroscopy (XPS), Auger electron spectroscopy (AES), secondary ion mass spectroscopy (SIMS), sputtered neutron mass spectrometry (SNMS), glow discharge optical emission spectroscopy/mass spectrometry (GD-OES/MS), new methods are still in demand because existing methods still have problems or inherent limitations. Either they are dependent on calibration procedures relying on standards that often do not exist (GD-OES/MS, XPS, AES, SIMS), or they are only vacuum compatible (*e.g.* SIMS, XPS, AES), or are difficult to use on non-conducting samples.

If nanometre and sub-nanometre in-depth resolution is necessary, the achievable resolution and sensitivity of existing techniques is not adequate. A comparison between several methods for depth profiling (XPS, SNMS, grazing incidence X-ray fluorescence (GI-XRF), Rutherford backscattering (RBS), total-reflection XRF (TXRF)) was performed, for

example, by Klockenkämper *et al.*⁴, showing that discrepancies of up to one order of magnitude in the parameters measured with different methods can occur, mainly due to calibration problems.

X-ray related methods like X-ray reflectivity (XRR),^{2,5–7} X-ray absorption or X-ray standing waves (XSW)^{8–27} are techniques that are suitable for a wide range of thin film and multilayer samples, and that have the potential to overcome some of the existing limitations. They do not require external standards, little or no sample preparation, and have short measuring times if they are used in combination with a synchrotron radiation source. In addition to a very high photon flux (orders of magnitude more than an X-ray tube) synchrotron radiation offers the advantage of precisely tunable photon energy up to several tens of keV.

XSW is rooted in the fact that incoming longitudinally coherent electromagnetic waves reflected at surfaces or interfaces interfere with the out-going reflected waves. Together they form a static intensity pattern that can be regarded as a ruler with subnanometre resolution. Although the XSW technique was developed *ca.* 40 years ago, it has only become really exploitable recently with the availability of high photon fluxes provided by second and third generation synchrotrons, such as ESRF,^{11,12,21,22} NLSL,^{9,14,16,20,23} APS,^{9,18} SRS,^{10,15} DELTA¹ or others.^{17,19,24,26,27}

XSW measurements are commonly performed around the Bragg angle of reflection^{9,11,12,17–20,23} or at normal incidence (NI-XSW).^{10,14,15,22} Multilayers^{13,17,18} or crystal lattices^{14,16} are subject to most of these investigations, which are well suited to characterize periodic structures. However, a periodicity in the sample (crystal lattice or periodic multilayer) is mandatory for these kinds of XSW measurements and limits its applicability. In contrary, X-ray standing waves at grazing incidence (GI-XSW)^{8,24–27}—also called long-period XSW—presented here require only one or several flat,

^a ISAS-Institute for Analytical Sciences, Bunsen-Kirchhoff-Str. 11, Dortmund, 44139, Germany. E-mail: kraemer@ansci.de

^b Department of Physics/DELTA, University of Dortmund, Maria-Goeppert-Mayer-Str. 2, Dortmund, 44221, Germany

reflecting interfaces and so-called marker atoms emitting detectable fluorescence radiation. Distances in a GI-XSW intensity pattern are in the range of nanometres and permit characterization of structures of this order of magnitude.

An XSW measurement procedure and a computer simulation program developed to calculate the XSW wavefield will be described in detail below.

Theoretical background

Beams of monochromatic and sufficiently longitudinally coherent X-ray radiation impinging onto and reflected at a sharp interface can interfere at their intersection point. Depending on the position of these intersection points relative to the mirror, constructive or destructive interference will occur, leading to a periodic pattern of nodes and antinodes of X-ray standing waves above the interface. Positions of minima and maxima only depend on angle of incidence and energy (wavelength) of the X-ray radiation. Marker atoms located at the position of a maximum will emit fluorescence radiation detectable by an energy dispersive detector. Positions of nodes and antinodes vary with varying angle of incidence and/or wavelength of the radiation,²⁸ thus changing the angle (as it was done in measurements presented here) or energy of the incoming beam results in a measurement of fluorescence *versus* angle or wavelength.

De Boer²⁹ and Klockenkämper³⁰ have outlined a method to calculate the XSW field above a surface or within a multilayer, utilizing formalisms introduced by Abelès³¹ and Parrat.³² This method has been expanded and implemented in a computer program that will be introduced in the following. Detailed calculation procedures are presented elsewhere.¹

To calculate the XSW field in a multilayer system the angle of incidence for each subsequent layer must be determined as a function of wavelength and refractive index of the layer material. Further, absorption inside each layer has to be considered. Dispersion and absorption coefficients for all elements and many compounds are tabulated or can be calculated.^{33,34} Then interference of the electrical fields of reflected and incoming beams in each layer are calculated under consideration of path length and phase for each beam. Squaring of the electrical field amplitudes delivers the field intensity. Marker atoms can probe the XSW field as they emit fluorescence radiation depending on their position inside the XSW field. Elements with absorption edge (*i.e.* binding energy) below the energy of the incident beam can serve as marker elements. Finally, taking into account absorption of emitted fluorescence radiation on its way to the detector one obtains the theoretical XSW signal.

In the following, the discussion of two examples will demonstrate the methodology. Fig. 1 shows the calculation of an XSW field above a flat silicon substrate for X-ray energy of 10 keV. Below the critical angle of Si (*i.e.* 0.18°) virtually no radiation penetrates the sample and interference of totally reflected and incoming beam lead to maxima of up to four times the intensity of the incident radiation I_0 . Above the critical angle, the field enters the substrate, resulting in a field intensity decreasing exponentially with depth. Oscillation amplitudes above the sample reduce to smaller values than below

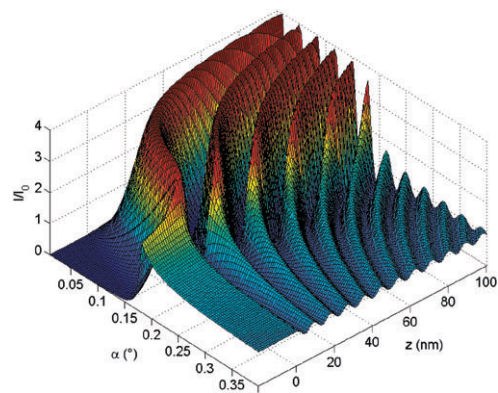


Fig. 1 Calculated XSW field above a Si substrate for $E = 10$ keV.

the critical angle. They average around 1 because less radiation is reflected at the interface leading to less intensity in the interference with the incident beam.

Fig. 2 displays the calculated XSW field for a 70 nm Si layer on a thick Ge substrate. The X-ray energy is again 10 keV. Similar to the pure Si substrate no radiation penetrates the sample for angles below the critical angle of Si. Above this angle and below the critical angle for Ge (*i.e.* 0.24°) radiation enters the Si layer. However, it is totally reflected at the Ge substrate. Partial internal reflection at the Si–vacuum interface leads to multiple inner reflections inside the Si layer. XSW field intensities far above $4I_0$ are produced due to coherent multi-reflections. Above the critical angle of Ge, radiation can penetrate the substrate, too, and the XSW field resembles the high angle region in Fig. 1 again.

Typically an XSW scan is performed by changing the angle of incidence by tilting the sample with the marker position kept constant. It can be extracted from the 3-dimensional graphs in Fig. 1 or Fig. 2 by plotting the cross-section of intensity *versus* angle at a fixed height value. If the marker is distributed throughout a layer of finite thickness integration of the whole layer has to be performed. This procedure and other possibilities of XSW scans are described in more detail elsewhere.¹

Experimental procedure

XSW measurements presented here were performed at beam-line BL 9 of the DELTA synchrotron facility^{35,36} in Dortmund

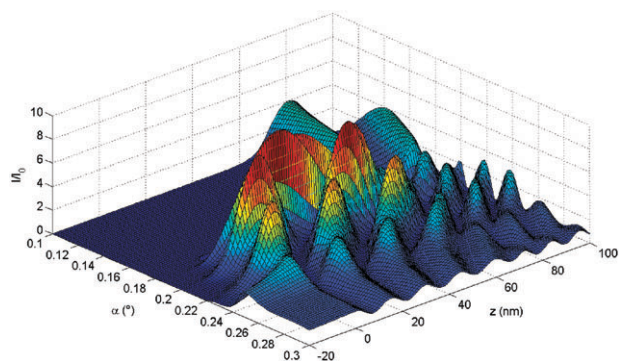


Fig. 2 Calculated XSW field for a 70 nm Si layer on a Ge substrate for $E = 10$ keV.

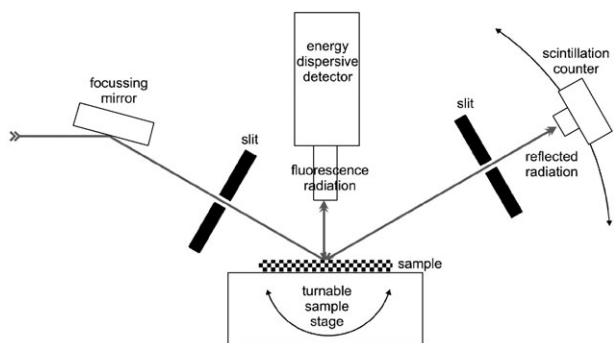


Fig. 3 Schematic set-up for XSW and reflectivity scans. Detailed explanations are given in the text.

(<http://www.delta.uni-dortmund.de/>) with energies of the incident beam between 13 keV (wavelength 0.0954 nm) and 15.2 keV (0.0816 nm) depending on the element utilized as a marker. Synchrotron radiation was generated by a superconducting asymmetric wiggler (SAW) and energy was monochromatized using a silicon (311) double crystal monochromator. Longitudinal coherence length ranged from 3.5 μm (15.2 keV) to 5.0 μm (13.0 keV). Detailed description of the beamline set-up can be found in Krywka *et al.*³⁷

The experimental set-up is displayed in Fig. 3. The beam was bent down and focused by a curved silicon mirror. The beam cross section (and thus the scanning region on the sample) was then defined by two slit systems in front of the sample to a width of 1 mm and a height of 150 μm . If necessary (to prevent damage to the detector) the beam intensity could be reduced by an absorber system. The angle of incidence on the sample was selected with an accuracy of 0.002° by tilting the sample stage. Fluorescence radiation from the sample was detected by an energy dispersive detector (XR-100CR, Amptek, Bedford, MA, USA) 1 cm perpendicular above the sample and processed by a multi-channel analyzer (MCA).

To perform an XSW scan, first an energy spectrum of the total fluorescence radiation at one angle of incidence is recorded and fluorescence intensity peaks of the marker element(s) of interest are located. Then regions of interest (ROIs) are allocated to channels comprising the peaks. Finally, an angle scan from 0.01° to approximately 0.6° is performed measuring the integrated intensity of each ROI *versus* the angle of incidence.

With the same set-up a reflectivity scan is performed using a scintillation counter approximately 1 m behind the sample at specular position (angle of incoming beam = angle of reflected beam) that is defined by another two slit system. This scan provides supplementary information on the sample and at the same time serves as a cross-check.

Analyzed samples and results

Layer thickness determination

Germanium layers on silicon (JENOPTIC, Jena, Germany) of four different thicknesses (29 nm, 76 nm, 309 nm and 1010 nm) were characterized with XSW scans at 15.2 keV. Fig. 4 shows measured and calculated curves for all analyzed samples. For

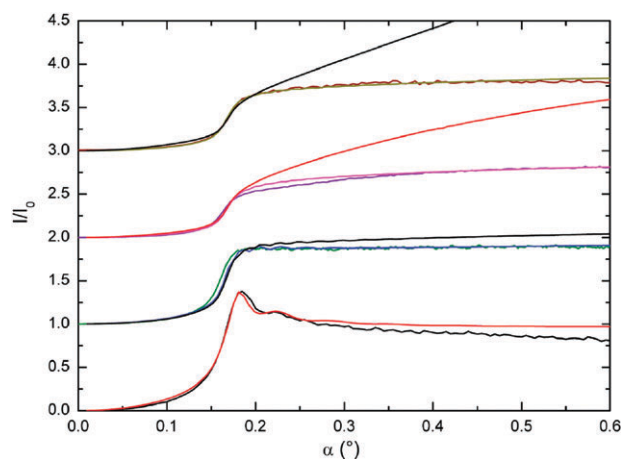


Fig. 4 XSW scans and fits for Ge layers on Si for different thicknesses (from top to bottom): 1010 nm, 309 nm, 76 nm, 29 nm. The curves are discussed in more detail in the text.

each thickness, the measured signal, a simulation fit for the nominal thickness and a best fit with varied thickness is shown. While the simulated curve for the thickness generally deviates from the other curves towards higher energies (with the exception of the thinnest Ge layer where the best fit leads to the nominal thickness), best fit and measurement curves can be distinguished by the noise affected appearance of the measurement curves. The thicknesses obtained by a best fit to the data shown here are (from top to bottom): 93 nm, 106 nm, 59 nm and 29 nm. It can be seen that deviations between the measured and simulated curve for the nominal thickness get very large for thicknesses above approximately 100 nm.

XSW oscillations are clearly visible for the thinnest film (29 nm) but virtually disappear for thicker layers because of high absorption inside germanium. Nevertheless, the shape of the XSW curve is still dependent on the thickness. A very good accordance of measured and calculated curves (accuracy about 2 nm) could be achieved for the 29 nm sample. Only for greater angles the measured signal falls below the calculated curve. This effect is even stronger for the 76 nm sample. Here the best fit turns out for a theoretical thickness of 57–60 nm. Dramatic deviations occur for the thicker samples. The theoretical intensity value approximately rises linearly for great angles as expected,³⁰ while the experimental value converges towards a horizontal asymptote. If the thickness in simulation is varied widely enough to fit the measurements it converges to a value of 102–110 nm for the 309 nm sample and 90–96 nm for the 1010 nm sample, respectively. Obviously thickness determinations cannot be performed with XSW at this energy for layers thicker than approximately 100 nm.

This can be understood regarding Fig. 5. The calculated XSW field inside a 100 nm Ge layer on Si for $E = 15.2$ keV (*cf.* Fig. 5a) shows clearly visible oscillations. The theoretical determination of the angle resolved fluorescence intensity requires integration over the entire 100 nm thickness of the Ge layer. Thus oscillations disappear in this averaging process (*cf.* Fig. 5b). Consequently, the nanometre sensitivity of XSW is lost, especially if the signal is additionally corrupted by noise and other errors. Obviously this method is most powerful if

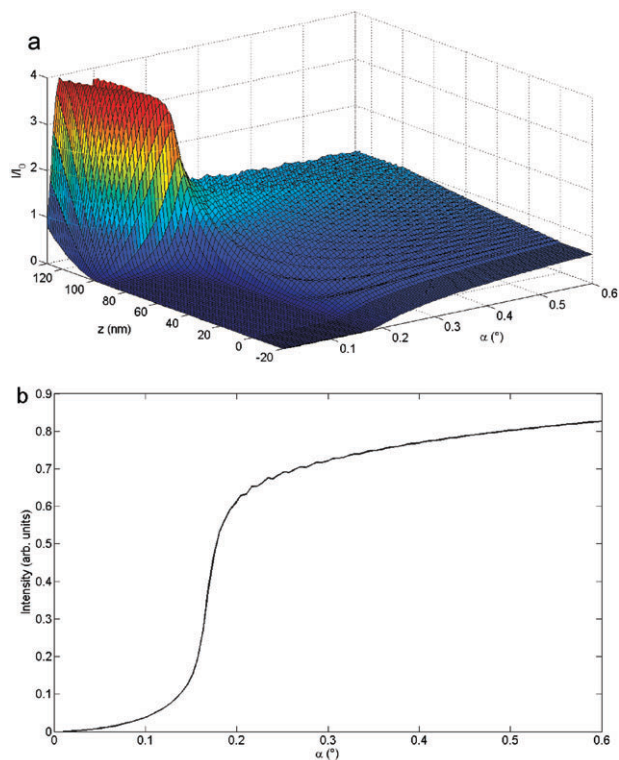


Fig. 5 XSW calculation for a 100 nm Ge on Si at $E = 15.2$ keV. (a) In the 3D visualization (above) of the XSW field (XSW intensity versus height above the substrate and angle of incidence) oscillations are clearly visible. (b) The angle scan (below) calculated by integrating the intensity of the entire Ge layer for each angle virtually shows hardly any oscillations.

the XSW period and the structures to be observed are in the same order of magnitude. As the oscillation period of XSW is proportional to the wavelength of the incident beam,^{1,24,25,30} it is possible to expand the accessible thickness range by reducing the photon energy. A lower limit for this energy is the binding energy E_B of the inner shell electron to be ejected by the incident photon that is always higher than the energy of the respective fluorescence radiation observed. For Ge $K\alpha$ fluorescence considered here, this limiting binding energy amounts to 11.103 keV. Thus, if 100 nm thickness may be regarded as the maximum thickness accessible at $E = 15.2$ keV, the total physical limit for Ge thickness determinations with XSW would be approximately 140 nm. However, marker elements with lower binding energies would permit much greater thicknesses. Finally utilizing $L\alpha$ fluorescence could offer access to greater thicknesses, but the energy of this fluorescence radiation is so low and thus absorption so high that XSW cannot occur.

Metal-organic multilayer

As an example of a metal-organic multilayer a complicated sample structure consisting of gold clusters on an 80 nm polystyrene film spin-coated on a Si/SiO₂ substrate was analyzed. If evaporation of gold is performed slowly enough, gold atoms do not form a continuous layer but nanometre sized

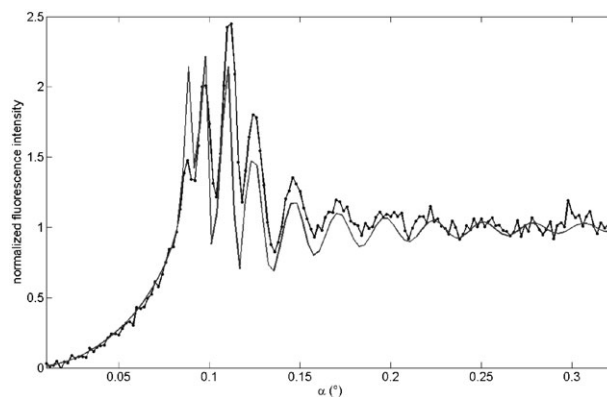


Fig. 6 XSW scan and fit for a polystyrene layer on Si/SiO₂ sample covered with Au clusters. Given values for the sample were 80 nm polystyrene thickness, 1 nm nominal gold thickness and silicon with a native oxide layer of unknown thickness. The fit curve was calculated for 1 nm gold on 80 nm polystyrene on 1 nm SiO₂ on silicon.

spherical clusters^{2,5} that allow incident radiation to partially pass even below the critical angle of reflection. On the other hand, the great optical contrast between gold and polystyrene leads to a strong and well structured XSW signal permitting an accurate fit (*cf.* Fig. 6). The fitted polystyrene and gold layer thicknesses (80 nm and 1 nm, respectively) coincide well with the nominal values determined through sputter rate (*i.e.* thickness of a homogeneously distributed gold layer with similar coating). The nominal thickness was confirmed by additional X-ray reflectivity measurements of the sample made during and after production.^{2,5,38}

Clearly, nominal gold thickness as it results from the simulation is an artificial concept. Reducing dispersion and absorption values (*i.e.* density of the specimen on the surface) increases the film thickness (*i.e.* the z -region where the gold is distributed) accordingly. The gold layer is not continuous, and a more appropriate measure than film thickness is surface coverage. Calculations⁵ for this sample deliver an area coverage of approximately 38%.

This value roughly corresponds to a film thickness of 3 times the nominal thickness and one third of the nominal dispersion and absorption coefficients, respectively. Input of these parameters into XSW simulation leads to a fit as satisfying as the one shown in Fig. 6.

Low-contrast organic mono- and double-layers

Fig. 7 shows an XSW scan of a biological layered sample. Phospholipids were deposited onto a quartz substrate to form Langmuir–Blodgett films³⁹ as mono- or double layers. A potassium chloride containing buffer solution is spread onto the Langmuir–Blodgett film. As the optical contrast between phospholipids and buffer is very low, only an element specific method can characterize the interface between the films. XSW can measure the signal of three elements simultaneously during one angle scan. Additionally to the phosphorus as a marker inside the phospholipid, chlorine and potassium as the main components of the buffer solution covering the phospholipid layer were measured. Strong background

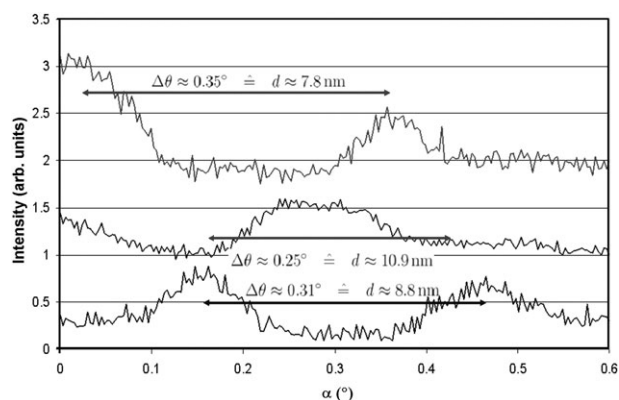


Fig. 7 Oscillating XSW signals for a phospholipid mono- or double-layer covered with KCl buffer solution. From top to bottom: Cl, K, P. Curves are shifted vertically for clarity. Oscillation periods are related to wavelength of the radiation and layer thickness by $\Delta\theta = \lambda/2d$.

scattering from the buffer solution made measurements difficult, but a periodic oscillation could be recorded for all elements. Knowing the wavelength of the incident radiation $\lambda = 0.0954$ nm ($E = 13.0$ keV) one can calculate a typical distance corresponding to the oscillation wavelengths that amount to 8–11 nm. The reliability is best for the P scan because for K and Cl the period could not be determined as precisely. With a typical phospholipid molecule chain length of 3 nm measurements suggest that the lipids form double or triple layers. However, the formation of a monolayer can be excluded. Alternatively, the measurements could suggest an amorphous phospholipid layer of 8–11 nm thickness.

Multilayers

A commercial multilayer laser mirror (Spectra-Physics, Mountain View, USA) was analyzed using TXRF and XSW techniques. TXRF showed Ti content in the mirror. However, light elements like C, Li, Si or Mg that are possibly incorporated in different layers were not accessible by this technique. In XSW measurement (*cf.* Fig. 8) again only the Ti signal

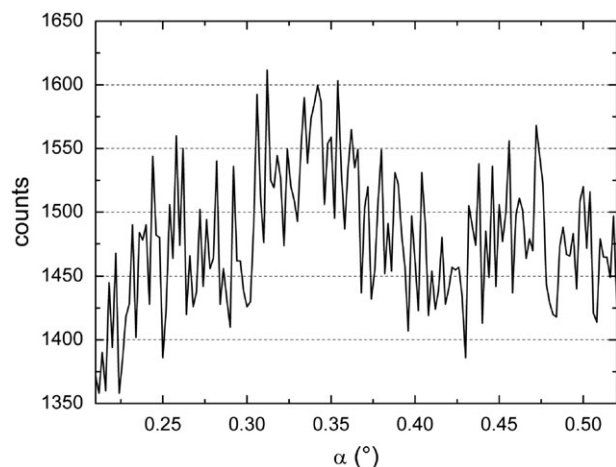


Fig. 8 XSW scan of a multilayer laser mirror, scanning of the Ti fluorescence signal.

Table 1 Calculated and measured layer thicknesses inside a multilayer laser mirror of alternating layers of TiO_2 and a second material (MgO, SiO_2 or LiF)

# TiO_2	# Second material	$d_{\text{th,ges}}$ (MgO)/nm	$d_{\text{th,ges}}$ (SiO_2)/nm	$d_{\text{th,ges}}$ (LiF)/nm	$d_{\text{exp,ges}}$ /nm
0	1	81.9	92.1	102.2	N/A
1	1	134.7	144.8	155.0	143.8
1	2	216.6	236.9	257.2	225.8
2	2	269.3	289.7	310.0	265.3
2	3	351.2	381.7	412.2	337.3
3	3	404.0	434.5	465.0	390.3
3	4	485.9	526.6	567.2	477.3

could be detected. However, together with the angle information—that is complementary to the element information obtained with TXRF—other materials can be characterized indirectly as will be shown below.

Fitting of the measurement shown in Fig. 8 with the XSW simulation program turned out to be too complicated because the layout of the sample (*i.e.* materials and number of layers) was not known. To extract information from the strongly noise-affected measurement a computer program was developed to calculate periodicities in the signal using fast Fourier transform algorithms.^{40–44} Transforming the frequencies of interest back to the angle space leads to an oscillation wavelength spectrum shown in Fig. 9.

From these angular periods and the wavelength of the synchrotron radiation used one can deduce the typical (multi-)layer thicknesses $d_{\text{exp,ges}}$ listed in the last column of Table 1. To obtain qualitative and quantitative information on the mirror one has to assume a sample structure. Typically, a laser mirror consists of several double layers of two materials. As TXRF measurements have proven Ti in the sample, titanium dioxide (TiO_2) is taken as one component; the second one must be a light element or compound, *e.g.* MgO, SiO_2 or LiF. Furthermore, each layer thickness must be 1/4 of the centre laser wavelength (*i.e.* 570 nm) for the mirror used divided by the known index of refraction n of the respective compound.⁴⁵ Table 1 lists the added thickness values of a periodic stack of alternating TiO_2 (52.8 nm) plus MgO (81.9 nm), SiO_2 (92.1 nm) or LiF (102.2 nm). It can be seen that theoretical and experimental values agree very well (only) for MgO as the second component together with TiO_2 . The table shows the summarized thickness of the sample region that a beam passes through if it is reflected at the first, second to the seventh

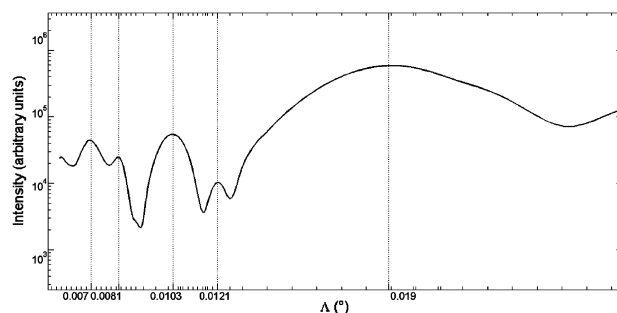


Fig. 9 Oscillation wavelength spectrum obtained from FFT of XSW scans on a multilayer laser mirror.

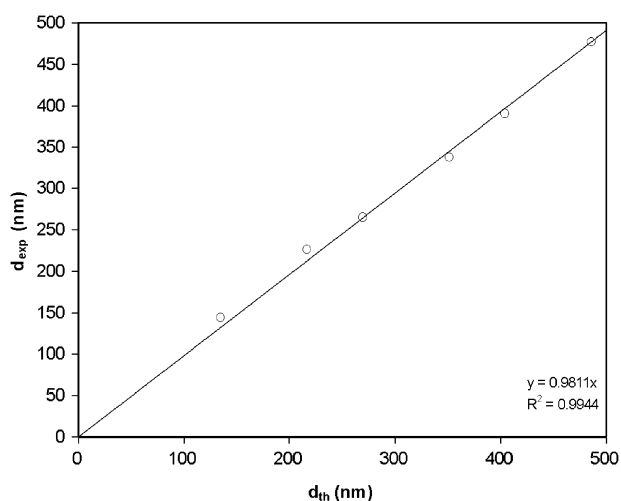


Fig. 10 Correlation of measured (ordinate) and calculated (abscissa) layer thicknesses in the multilayer mirror.

interface. The very first layer is not visible because its small thickness corresponds to a long oscillation wavelength located inside the very broad maximum beyond the great angle limit in Fig. 9.

Fig. 10 displays the correlation of the expected and measured thicknesses inside the multilayer mirror of TiO_2 and MgO . The coincidence of the values is obvious. Thus, XSW-method has been proven to be capable of determining composition and thicknesses of an unknown multilayer sample in just one scan.

Conclusions

It has been shown that X-ray standing waves are a versatile and powerful tool to analyze layered structures on a nanometre scale, both concerning distances/layer thicknesses and element determination and distribution. A necessary requirement for these kinds of analysis is a flat, smooth surface; however, different types of sample ranging from liquid to solid, non-conducting to conducting, monolayer to periodic multilayer systems can be analyzed. The versatility of the method has been demonstrated with 4 different types of samples.

Germanium layer thicknesses on a silicon substrate could be measured in a range below 100 nm. Increasing thickness of the layer corrupted the signal more and more. However, as has been shown, the accessible thickness range can be expanded by moving to longer wavelengths.

A sample of gold clusters on a polystyrene film was characterized qualitatively and quantitatively. Incorporating heavy marker atoms, a weakly absorbing matrix and dimensions in the nm range, XSW measurements appear to be ideal for this technologically important kind of sample.

Only few methods are sensitive to low contrast interfaces especially in biological samples that are of increasing importance in life science. As has been shown, XSW can deliver—in certain limits—even quantitative thickness information using marker elements already incorporated in the materials under investigation.

Finally, a complicated periodic multilayer structure—in this case a laser mirror—can be analyzed qualitatively and quantitatively. Combined with a fast Fourier transform algorithm and general information about laser multilayer mirrors, the advantages of XSW (element sensitivity, periodicity and nm resolution) can be exploited.

Limits of XSW methods have come visible during this work, too. Very thick layers (*e.g.* Ge samples) or strongly scattering materials (like buffer solution in biological samples) can cause problems. Some might be reduced by changing experimental parameters like the wavelength of photon flux or by sample preparation. A marker positioned at a characteristic location in the sample is essential for XSW measurements. Thus, samples not fulfilling these conditions cannot be analyzed until a marker is added to the system. Further, generating a theoretical curve fitting to the measurements gets increasingly difficult with the number of unknown parameters. On the other hand, well known system structures can be analyzed quickly, easily and accurately if only one or few parameters have to be adjusted.

In the future other scanning variables can be utilized (*e.g.* varying the energy of the incoming beam with a monochromator), which open new approaches and possibilities.

Due to the need for high photon fluxes and the tunability of the energy, XSW is a typical synchrotron technique. Nonetheless, XSW has been proven to be a versatile technique which can be employed in a wide variety of problems which otherwise are difficult to tackle.

Acknowledgements

The financial support by the Ministerium für Innovation, Wissenschaft, Forschung und Technologie des Landes Nordrhein-Westfalen and by the Bundesministerium für Bildung und Forschung is gratefully acknowledged. We would also like to thank Simone Streit, Experimental Physics I, University of Dortmund, for providing the gold polymer sample together with helpful data, and Jessica Irrgang, Biological-Chemical Microstructure Technology, University of Dortmund, for preparation of and information about the phospholipid layers. The authors thank the DELTA machine group for providing the synchrotron radiation and technical support. C. S. would like to acknowledge M. Tolan for supporting this work.

References

- 1 M. Krämer, A. v. Bohlen, C. Sternemann and R. Hergenröder, *Appl. Surf. Sci.*, 2006, DOI: 10.1016/j.apsusc.2006.07.076.
- 2 R. Weber, *Dissertation*, Christian-Albrechts-Universität, Kiel, 2002.
- 3 C. P. Wong, *Polymers for Electronic and Photonic Applications*, Academic Press, Boston, 1993.
- 4 R. Klockenkamper, H. W. Becker, H. Bubert, H. Jenett and A. von Bohlen, *Spectrochim. Acta, Part B*, 2002, **57**, 1593–1599.
- 5 M. Krämer, *Diploma thesis*, University of Dortmund, Dortmund, 2003.
- 6 J. Stettner, *Dissertation*, Christian-Albrechts-Universität, Kiel, Germany, 1995.
- 7 M. Tolan, *X-Ray Scattering from Soft Matter Thin Films – Materials Science and Basic Research*, Springer-Verlag, Berlin, 1999.

- 8 M. Caffrey and J. Wang, *Annu. Rev. Biophys. Biomol. Struct.*, 1995, **24**, 351–377.
- 9 L. W. Cheng, P. Fenter, N. C. Sturchio, Z. Zhong and M. J. Bedzyk, *Geochim. Cosmochim. Acta*, 1999, **63**, 3153–3157.
- 10 V. R. Dhanak, A. G. Shard, S. D'Addato and A. Santoni, *Chem. Phys. Lett.*, 1999, **306**, 341–344.
- 11 M. Drakopoulos, J. Zegenhagen, T. L. Lee, A. Snigirev, I. Snigireva, V. Cimalla and O. Ambacher, *J. Phys. D: Appl. Phys.*, 2003, **36**, A214–A216.
- 12 M. Drakopoulos, J. Zegenhagen, A. Snigirev, I. Snigireva, M. Hauser, K. Eberl, V. Aristov, L. Shabelnikov and V. Yunkin, *Appl. Phys. Lett.*, 2002, **81**, 2279–2281.
- 13 S. K. Ghose and B. N. Dev, *Phys. Rev. B: Condens. Matter Mater. Phys.*, 2001, **63**, 5409.
- 14 T. Jach, Y. Zhang, R. Colella, M. de Boissieu, M. Boudard, A. I. Goldman, T. A. Lograsso, D. W. Delaney and S. Kycia, *Phys. Rev. Lett.*, 1999, **82**, 2904–2907.
- 15 R. G. Jones, A. S. Y. Chan, M. G. Roper, M. P. Skegg, I. G. Shuttleworth, C. J. Fisher, G. J. Jackson, J. J. Lee, D. P. Woodruff, N. K. Singh and B. C. C. Cowie, *J. Phys.: Condens. Matter*, 2002, **14**, 4059–4074.
- 16 T. L. Lee and M. J. Bedzyk, *Phys. Rev. B: Condens. Matter Mater. Phys.*, 1998, **57**, R15056–R15059.
- 17 A. Lessmann, M. Schuster, H. Riechert, S. Brennan, A. Munckholm and G. Materlik, *J. Phys. D: Appl. Phys.*, 1999, **32**, A65–A70.
- 18 D. L. Marasco, A. Kazimirov, M. J. Bedzyk, T. L. Lee, S. K. Streiffer, O. Auciello and G. R. Bai, *Appl. Phys. Lett.*, 2001, **79**, 515–517.
- 19 S. Nakatani, K. Sumitani, A. Nojima, T. Takahashi, K. Hirano, S. Koh, T. Irisawa and Y. Shiraki, *Jpn. J. Appl. Phys., Part 1*, 2003, **42**, 7050–7052.
- 20 G. Scherb, A. Kazimirov, J. Zegenhagen, T. L. Lee, M. J. Bedzyk, H. Noguchi and K. Uosaki, *Phys. Rev. B: Condens. Matter Mater. Phys.*, 1998, **58**, 10800–10805.
- 21 F. Schreiber, K. A. Ritley, I. A. Vartanyants, H. Dosch, J. Zegenhagen and B. C. C. Cowie, <http://www.esrf.fr/info/science/highlights/2001/surfaces/SURF1.html>.
- 22 F. Schreiber, K. A. Ritley, I. A. Vartanyants, H. Dosch, J. Zegenhagen and B. C. C. Cowie, *Surf. Sci. Lett.*, 2001, **486**, L519.
- 23 B. P. Tinkham, D. M. Goodner, D. A. Walko and M. J. Bedzyk, *Phys. Rev. B: Condens. Matter Mater. Phys.*, 2003, **67**, 5404–5404.
- 24 T. P. Trainor, A. S. Templeton, G. E. Brown and G. A. Parks, *Langmuir*, 2002, **18**, 5782–5791.
- 25 T. P. Trainor, A. S. Templeton and P. J. Eng, *J. Electron Spectrosc. Relat. Phenom.*, 2006, **150**, 66–85.
- 26 J. Wang, M. Caffrey, M. J. Bedzyk and T. L. Penner, *J. Phys. Chem.*, 1994, **98**, 10957–10968.
- 27 J. Wang, M. Caffrey, M. J. Bedzyk and T. L. Penner, *Langmuir*, 2001, **17**, 3671–3681.
- 28 R. T. Zhang, R. Itri and M. Caffrey, *Biophys. J.*, 1998, **74**, 1924–1936.
- 29 D. K. G. de Boer, *Phys. Rev. B: Condens. Matter*, 1991, **44**, 498–511.
- 30 R. Klockenkämper, *Total-Reflection X-ray Fluorescence Analysis*, John Wiley & Sons, New York, 1996.
- 31 F. Abelès, *Ann. Phys.*, 1950, **12**, 596–640, 706–782.
- 32 L. G. Parrat, *Phys. Rev.*, 1954, **95**, 359–369.
- 33 CXRO, http://www.cxro.lbl.gov/optical_constants/.
- 34 B. L. Henke, E. M. Gullikson and J. C. Davis, *At. Data Nucl. Data Tables*, 1993, **54**, 181–342.
- 35 Dortmunder Elektronen Speicherring Anlage, <http://www.delta.uni-dortmund.de/>.
- 36 M. Tolan, T. Weis, K. Wille and C. Westphal, *Synchrotron Radiat. News*, 2003, **16**, 9–11.
- 37 C. Krywka, M. Paulus, C. Sternemann, M. Volmer, A. Remhof, G. Nowak, A. Nefedov, B. Pöter, M. Spiegel and M. Tolan, *J. Synchrotron Radiat.*, 2006, **13**, 8–13.
- 38 S. Streit, private communication.
- 39 K. B. Blodgett and I. Langmuir, *Phys. Rev.*, 1937, **51**, 964–982.
- 40 J. W. Cooley and J. W. Tukey, *Math. Comput.*, 1965, **19**, 297–301.
- 41 P. Duhamel and M. Vetterli, *Signal Process.*, 1990, **19**, 259–299.
- 42 M. Frigo and S. G. Johnson, *Proceedings of International Conference on Acoustics Speech, and Signal Processing*, 1998, 1381–1384.
- 43 A. V. Oppenheim and R. W. Schaffer, *Discrete-Time Signal Processing*, Prentice-Hall, Upper Saddle River, NJ, 1989, 611, 619.
- 44 C. M. Rader, *Proc. IEEE*, 1968.
- 45 LOT-Oriel Group Europe, <http://www.lot-oriel.com>.